24th Australasian Fluid Mechanics Conference – AFMC2024
Canberra Australia
1-5 December 2024
Paper No: AFMC2024-99

Modelling the dispersion of traffic pollutants in a real-world street canyon with unevenly distributed trees

Lehan Chen [1], Chao Mai [1], Yuhan Huang [1,*], Arezoo Shirazi [2], Nimish Biloria [2], Leena Thomas [2]

[1] Centre for Green Technology, School of Civil and Environment Engineering, University of Technology Sydney, Ultimo NSW 2007, Australia
[2] School of Built Environment, University of Technology Sydney, Ultimo NSW 2007, Australia
* Email: Yuhan.Huang@uts.edu.au

Abstract

Vehicle emissions are a major source of roadside air pollution, particularly in urban street canyons where driveways are close to sidewalks. This paper investigates pollutant dispersion in a real-world urban canyon of Harris Street in the Sydney CBD, which includes unevenly distributed trees - a factor that has been rarely considered in the literature but is prevalent in the real-world. Experiments were conducted to measure traffic volumes and roadside pollutant concentrations using a camera and low-cost air quality sensors, which provided data for model setup and verification. Large eddy simulation and porous media model were used to explore the effects of the tree canopies on NO_2 dispersion. Results show that when the tree canopies are unevenly spaced and sized, air pollutants preferentially disperse horizontally, creating pollution hotspot zones at the intersections on both ends of the road. In the absence of the tree canopies (an imagined case), the horizontal transport of pollutants would be greatly reduced, leading to more concentrated pollution within the street. This could reduce the air quality at intersections to one-tenth of the current levels. The results indicate that the presence of irregular tree canopies significantly impacts the horizontal movement of air pollutants, shifting pollution hotspots from within the street towards street intersections and thus posing a greater health risk to a larger number of pedestrians.

1. Introduction

Major outdoor air pollution sources include residential energy for cooking and heating, vehicles, power generation, agriculture/waste incineration, and industry. Among them, road transportation is usually regarded as the single largest source of atmospheric pollutants in cities (Sá *et al.*, 2022). Motor vehicle emissions are an important factor in street-level air quality, especially in urban street canyon environments where driveways are in close proximity to sidewalks, and the time and amount of human inhalation of the tailpipe exhaust are greatly increased (Xie *et al.*, 2020).

In recent years, an increasing number of studies on roadside trees have focused on factors of tree shapes and crown heights (Guo *et al.*, 2023), and used simplified 2D models (Huang *et al.*, 2019) to simulate the impact of street trees on pollutant dispersion. In reality, tree distribution along streets is often asymmetrical due to factors such as varying survival rates, planting and replacement practices, and urban infrastructure layout. Trees may die or be removed, creating gaps, and new plantings may vary in species and size. Additionally, trees might be removed for construction projects, such as bus stations, further contributing to this asymmetry. However, this tree distribution factor has been rarely mentioned in the literature but is commonly seen in the real-world. Considering these real-world

conditions, this study aims to numerically investigate the dispersion process of traffic pollutants along a street canyon with unevenly distributed trees to help urban planners more effectively address traffic pollutant dispersion and public exposure issues.

2. Methodology

2.1 Experimental background

To validate the model, a seven-day field experiment was conducted on Harris Street, Sydney, which is located in the city center with very high traffic and pedestrian activities. This street is a one-way road with five lanes running northwest. The street is flanked by trees with uneven distribution, and a pedestrian bridge connects the buildings on both sides of the street. Hibou air quality monitoring sensors were installed at two observation points in the street (Figure 1): Point 1 was at the entrance of the pedestrian bridge, and Point 2 was set on the sidewalks, 1.7 meters above the ground directly below Point 1. Additionally, a camera was placed in the middle of the footbridge to continuously take a video of the passing vehicles, and an image processing algorithm was used to obtain the traffic flow volume of each lane. These data were used to setup and verify the emission dispersion model.

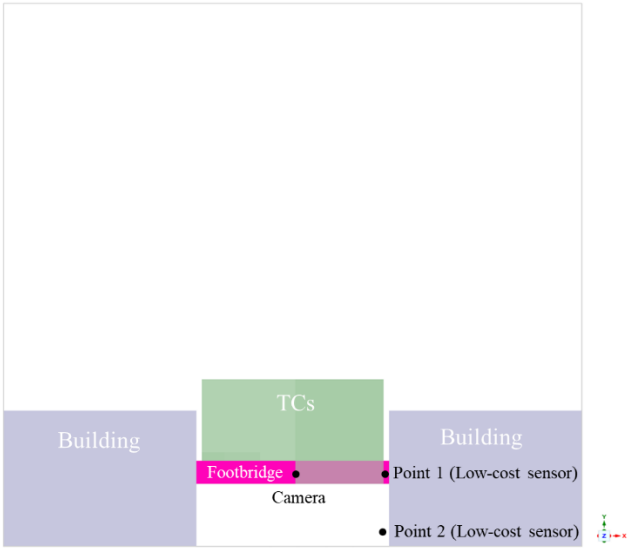

Figure 1. A schematic of the studied urban street canyon and the installation of low-cost air quality sensors.

2.2 Geometry of the street canyon

Considering that the urban environment is an extremely complex set of physical phenomena, the simulation must be abstracted into conceptual models (Tominaga *et al.*, 2023). Figure 2 shows a top view of the geometric model used for this study. The buildings are the same size, with a height H = 13 m, a width of W = 17.5 m and a length of L = 180 m. The size of the whole computational domain is $H_s = 4H$, $W_s = 3W$, $L_s = 1.05L$. Five lanes of line sources are used to model pollution sources. Trees are asymmetrically placed on two sides along the street, as shown in Figure 2, representing the real-world situation. Trees and footbridge are two of the most distinctive features the street. The tree canopy (TC) model (Mochida *et al.*, 2008) is used in this research. This simplification is one of the most commonly used methods for assessing the impact of trees on the urban outdoor microclimate. The tree trunk is neglected, and the tree canopy is considered a porous medium (Li *et al.*, 2023a), which is of the similar height as the nearby building. The tree canopy covers 50% of the area along the length of the roadway. The bottom of tree canopies is 6 meters above the ground, and the canopies

are 10 meters high. They are scattered asymmetrically on both sides of the street, with certain portions of the tree crowns covering the entire street (i.e., TC4 in Figure 2).

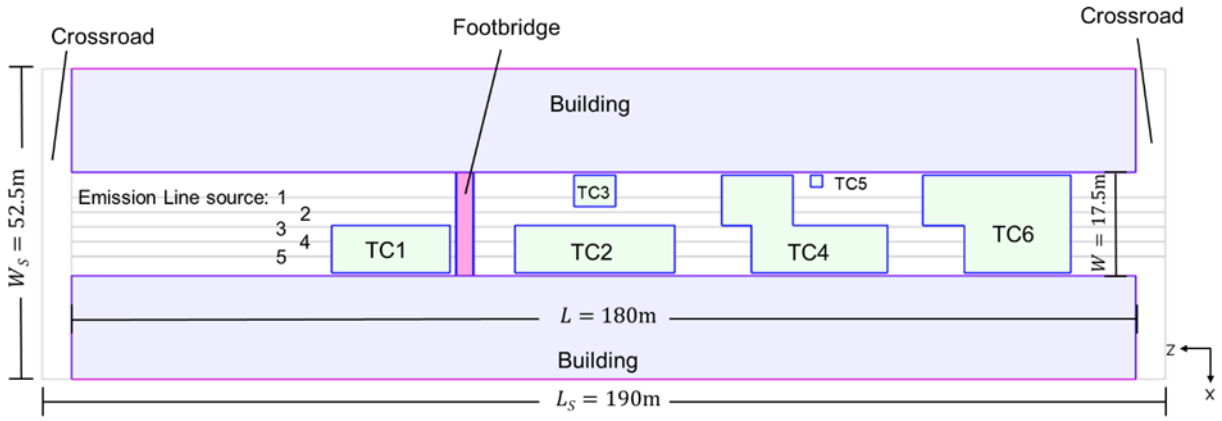

Figure 2. Top view of the geometric model.

2.3 Treatment of trees

Research has shown that LES models for simulating airflow and pollutant dispersion in urban canyons well agreed with wind tunnel experiments (Xie *et al.*, 2020). LES uses filtered Navier-Stokes equations and is suitable for more complex geometries than RANS. The flow profiles of turbulent kinetic energy (k) are imposed at the inlet plane by the Atmospheric Boundary Layer using eq. (1) (Xue & Li, 2017):

$$k(y) = \frac{(u^*)^2}{\sqrt{C_\mu}} \tag{1}$$

where $u^* = 0.52$ is the friction velocity, $\kappa = 0.41$ is the von Karman constant, and $C_\mu = 0.09$ is an empirical constant. Turbulence dissipation rate (ε) is imposed at the inlet by eq. (2):

$$\varepsilon(y) = \frac{(u^*)^3}{\kappa(y+y_0)} \tag{2}$$

For the tree canopy, the porous media model is utilized (Fu *et al.*, 2024). Eq. (3) is used to calculate the inertial resistance source term of the tree canopy:

$$S_i = -(\frac{\mu}{\alpha} v_i + C_u \frac{1}{2} \rho |v| v_i) \tag{3}$$

where S_i is the source term for the i^{th} (x, y, or z direction) momentum equation, α is the permeability, $|v|$ is the magnitude of the velocity and C_u is the inertial resistance coefficient. As the Reynolds number of the flow increases, inertial forces become more significant and the viscous loss term can be ignored (Zhang *et al.*, 2022). Thus, the inertial resistance source term can be simplified to eq. (4):

$$S_i = -C_u \frac{1}{2} \rho |v| v_i \tag{4}$$

where C_u is expressed as eq. (5) (Li *et al.*, 2023b; Wilson, 1985):

$$C_u = 2 L_{AD} C_d \tag{5}$$

Previous studies have shown that the Leaf Area Density (L_{AD}) and drag coefficient (C_d) depend on vegetation species (Xue & Li, 2017). For the summer season, an average value of C_d and L_{AD} are 0.25 and 1.6 m^2 m^{-3} respectively for the tree canopy (Jeanjean *et al.*, 2017). The parasol trees on both sides of Harris street belong to deciduous trees, and the averaged inertial resistance coefficient of the experimental deciduous trees was 0.712 (Ha *et al.*, 2019).

The deposition effect of tree canopy is influenced by three factors, namely L_{AD}, deposition velocity

(v_d) and local pollution concentration (C). Consequently, a concentration source term is used to model this impact, as calculated by eq. (6) (Xue & Li, 2017):

$$S_C = -L_{AD} v_d C \tag{6}$$

According to Grylls & van Reeuwijk (2021), typical v_d values are less than 0.01 m/s for most pollutants and tree species. Considering the parameter ranges and experimental setting in previous studies (Xue & Li, 2017), v_d = 0 is in accordance with the wind tunnel dataset (CODASC, 2008), which is used to validate the aerodynamic model in this work.

2.4 Model setup

Meteorology data (NSW Bureau of Meteorology, 2023) was used to set up the inlet conditions. The studied street had south-west winds throughout the test period (i.e., winds are perpendicular to the street). The mean velocity is 6 m/s at the reference height H. Flow profiles of mean wind speed (U) was expressed using eq. (7) (Xue & Li, 2017):

$$U(y) = \frac{u^*}{\kappa} \ln\left(\frac{y+y_0}{y_0}\right) \tag{7}$$

Fluctuation is produced using the vortex method. The wind temperature is 293 K. The total exhaust flow rate was estimated to be 1229.54 g/mile per vehicle by the EMFAC emission model (California Air Resources Board, 2023). Because the traffic volume varies among lanes, the emission source rate of each lane is set up separately, as shown in Table 1.

Emission source	Average number of vehicles per minute	Mass flow rate (kg/s)
Lane 1	7.438	6.314×10^{-3}
Lane 2	7.409	6.289×10^{-3}
Lane 3	12.552	1.066×10^{-2}
Lane 4	15.702	1.333×10^{-2}
Lane 5	14.589	1.238×10^{-2}

Table 1. Set up of emission source rates.

The mass fractions for NO, NO_2, and CO_2 are 5.72×10^{-6}, 1.3×10^{-3}, and 9.95×10^{-1}, respectively. The exhaust temperature is 578 K. The top and lateral sides of the computational domain were configured as free-slide walls (Li *et al.*, 2023b). A constant static gauge pressure of 0 Pa is used at the outlet plane (Zheng & Yang, 2022). The time step size is 0.2 s, with up to 20 iterations per time step. After 1500 steps for physical initialization time, the last 500 steps of simulation data were used for analysis.

2.4 Grid independence and model verification

Three meshes with different grid densities are tested to achieve mesh independence. All meshes adopted poly-hexacore cells, with 0.57, 1.83, and 3.00 million cells for coarse, medium and fine, respectively. Figure 3 shows the variation curves of velocity and NO_2 molar fraction of Point 2 over time. As shown in Figure 3(a), the velocity at Point 2 remains almost constant after 400 s. The velocity of the coarse grid remains at 1.5 m/s, but the velocities of the medium and fine grids remain at 1 m/s with almost identical fluctuation patterns. Similarly, as shown in Figure 3(b), the molar concentration at point 2 remains almost constant after 400 s, and the fluctuation patterns of the medium and fine grids are nearly the same. The results in Figure 3 indicate that when the grid number reaches the medium level or above, the simulation results are independent of the grid density. This also indicates that the modelled flow has been fully developed after 400 s, allowing for result analysis.

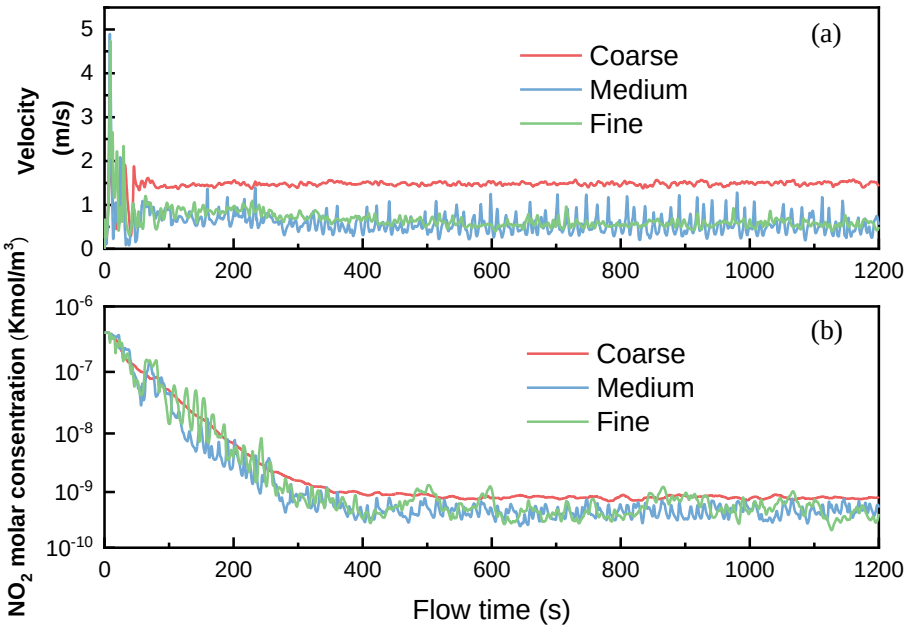

Figure 3. Grid independence verification of (a) velocity and (b) NO_2 molar concentration at Point 2.

The Mean and RMS values between different grids after 400s are calculated in Table 2. It can be seen that the Mean velocities at the point for the medium and fine grids are nearly identical, at 0.57 and 0.59 respectively, while the coarse grid yields a value of 1.49, approximately three times that of the other two grids. The mean NO_2 concentration at this location exhibits a similar pattern, with the medium and fine grid values being 4.55 and 5.21, and the coarse grid values reaching 1.53 and 1.75 times those of the other two grids. The RMS values for the medium and fine grids at this point are similar and greater than that for the coarse grid. This is because the larger cell size of the coarse grid tends to neglect the presence of smaller eddies when using LES. In contrast, smaller grid sizes capture more complex eddies, leading to fluctuations in the velocity and concentration values at this location. However, these fluctuations are within a small range, and the amplitude and frequency of the fluctuations for the medium and fine grids are similar, indicating grid convergence. Since the computation time of the fine grid is twice that of the medium grid, the medium grid is used for the subsequent simulations.

	Coarse		**Medium-**		**Fine**	
	Mean	**RMS**	**Mean**	**RMS**	**Mean**	**RMS**
Velocity	1.49	1.532	0.59	0.554	0.57	0.71
NO_2	7.99×10^{-10}	1.83×10^{-10}	4.55×10^{-10}	5.14×10^{-10}	5.21×10^{-10}	4.75×10^{-10}

Table 2. A quantitative assessment of mean and rms for three grid.

To validate the model, the calculated NO_2 molar concentrations are compared against the experimental data of the two observation points. Figure 4 shows the experimental and simulated NO_2 molar concentrations along a vertical line that passes through the two observation points (i.e., Line: $x = \frac{2}{3}W_S, z = \frac{1}{3}L_S,\ y = (0\ to\ 1)\ H_S$). As shown in Figure 4, the simulation results agree well with the experimental results at both Points 1 and 2. They are of the same order of magnitude. Therefore, the model is considered accurate for this study.

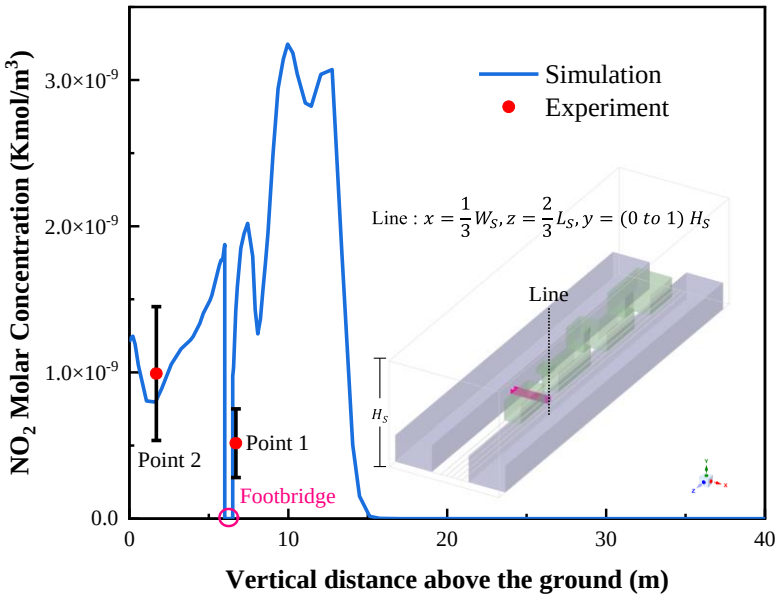

Figure 4. Comparison of measured and modelled NO_2 molar concentrations at Points 1 and 2.

3. Results and discussion

Figure 5(a) shows the streamline and NO_2 distribution in a cross-section (x-y plane) of TC1 within the street canyon, and Figure 5(b) presents these distributions in the same plane without TC (i.e., an imagined case for comparison). Comparing the streamlines, the near-ground velocity in Figure 5(b) without TC is about twice that of Figure 5(a) with TC. In Figure 5(a), the reduced air ventilation causes pollutants to linger near the ground longer. The streamlines indicate that airflow in Figure 5(b) moves more smoothly and quickly into the upper atmosphere compared to Figure 5(a). This matches the concentration contour, where NO_2 in Figure 5(b) accumulates in the center of the street canyon, while the NO_2 in Figure 5(a) gathers near the ground on the leeward side due to TC1. This means that TC significantly impacts pollutant hotspot distribution, shifting hotspots to unobstructed areas.

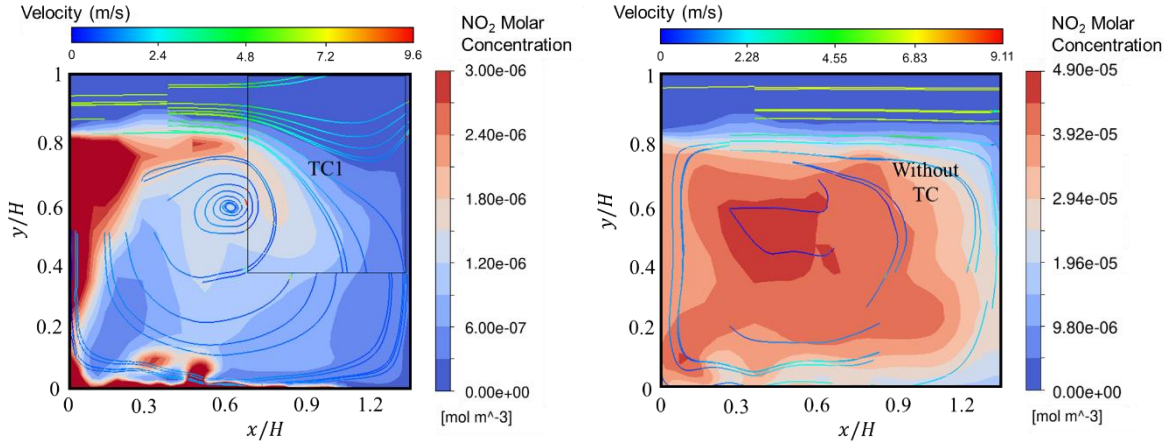

Figure 5. Cross-sectional distributions of NO_2 molar concentrations and streamlines in the street canyon: (a) with TC presence (the real-word case); (b) in the same location without TC (an imagined case).

To better study the horizontal dispersion of pollutants along the street, the two vertical planes that pass through Line 1 (Plane 1, y-z plane at x =1/3W_S) and Line 2 (Plane 2, y-z plane at x =2/3W_S)

were selected for analysis. Figure 6 illustrates the NO_2 concentration and streamline distributions on these two planes for both with (Figure 6(a)) and without (Figure 6(b)) TCs. A comparison of the streamlines reveals that the airflow in Figure 6(a) exhibits a 45° upward inclination with a horizontal velocity component, whereas the airflow in Figure 6(b) is predominantly vertical. This means that the unevenly distributed TCs alter the pollutant dispersion pattern, preventing it from escaping into the upper atmosphere and instead promoting horizontal dispersion through the gaps between them. The NO_2 concentration contours further corroborate this observation: NO_2 with TCs are more concentrated at both ends of the street, indicating that TCs facilitate the horizontal dispersion of pollutants to the more open intersections. These findings demonstrate that the presence of unevenly distributed trees significantly influences pollutant distribution and diffusion direction, increasing horizontal dispersion and resulting in pedestrians waiting at intersections inhaling harmful gases that are ten times or more than a street with no trees.

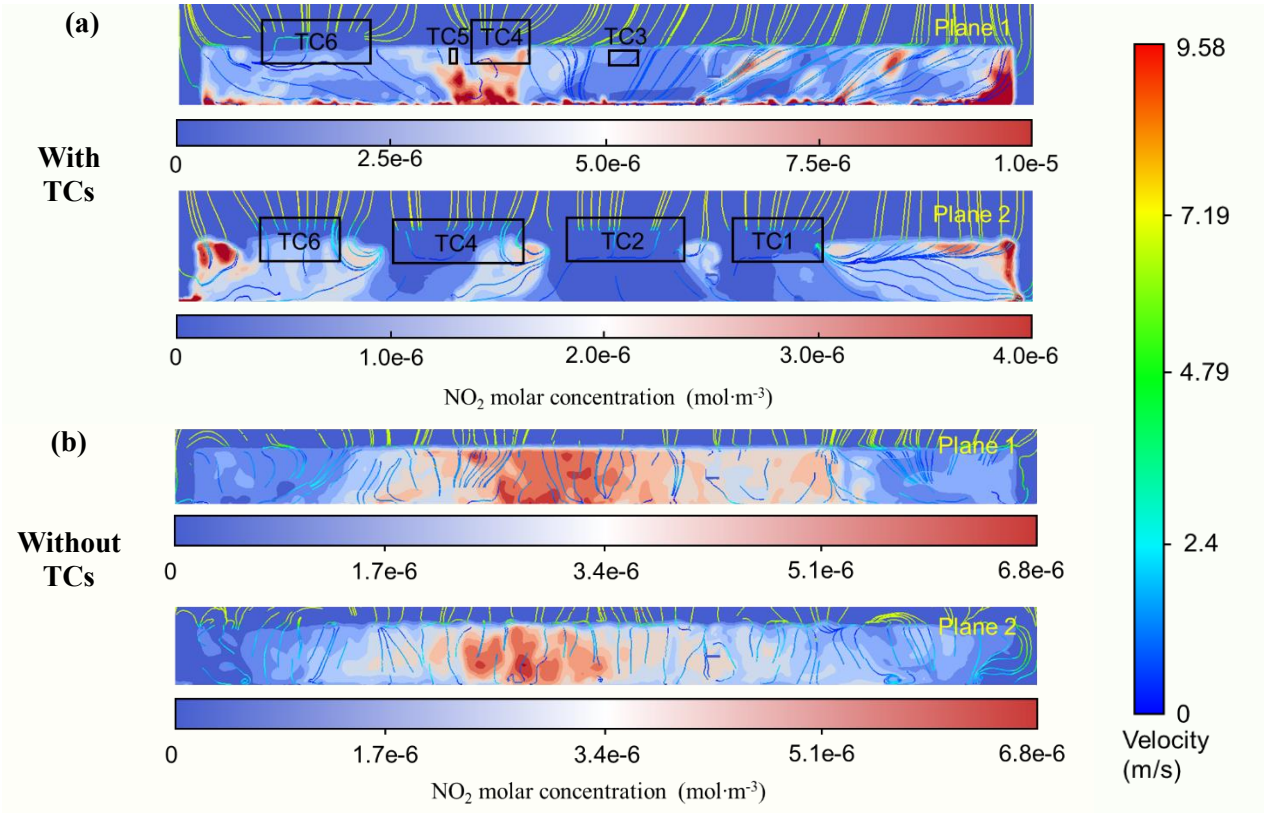

Figure 6. Distribution NO_2 molar concentrations ($mol \cdot m^{-3}$) and streamlines of Planes 1 and 2 (y-z plane).

4. Conclusion

This paper simulated the dispersion patterns of traffic pollutants in a real street canyon with asymmetrically distributed tree canopies. Results show that, when the roadside tree canopies are unevenly spaced and sized, air pollutants preferentially disperse in the horizontal direction, creating pollution hotspot zones at the intersections. However, in the ideal scenario without trees, the horizontal dispersion of pollutants is greatly reduced. As a result, the pollutant concentration at the intersection is significantly reduced to about one-tenth of that with trees. This indicates that unevenly distributed tree canopies within the street have a substantial impact on the horizontal dispersion of pollutants. Consequently, pedestrians waiting at intersections are exposed to much higher air pollution compared to those within the street (e.g., on the footbridge), impacting a larger population. This study provides valuable insights for urban planners in making decisions to reduce human exposure to

traffic-related emissions.

Acknowledgments

This project was supported by the Cross Faculty Collaboration Scheme of the UTS Faculty of Design, Architecture and Design. Y.H. is a recipient of the ARC Discovery Early Career Research Award (DE220100552).

References

California Air Resources Board. 2023. *EMFAC Emissions Inventory*.

CODASC. 2008. *Concentration data of street canyon*.

Fu, R., Pađen, I., & García-Sánchez, C. 2024. Should we care about the level of detail in trees when running urban microscale simulations? *Sustainable Cities Soc.*, *101*, 105143.

Grylls, T., & van Reeuwijk, M. 2021. Tree model with drag, transpiration, shading and deposition: Identification of cooling regimes and large-eddy simulation. *Agric. For. Meteorol.*, *298–299*, 108288.

Guo, Y., Xiao, Q., Ling, C., Teng, M., Wang, P., Xiao, Z., & Wu, C. 2023. The right tree for the right street canyons: An approach of tree species selection for mitigating air pollution. *Build. Environ.*, *245*, 110886.

Ha, T., Lee, I., Hong, S.-W., & Kwon, K.-S. 2019. CFD assisted method for locating and processing data from wind monitoring systems in forested mountainous regions. *Biosyst. Eng.*, *187*, 21–38.

Huang, Y., Li, M., Ren, S., Wang, M., & Cui, P. 2019. Impacts of tree-planting pattern and trunk height on the airflow and pollutant dispersion inside a street canyon. *Build. Environ.*, *165*.

Jeanjean, A. P. R., Buccolieri, R., Eddy, J., Monks, P. S., & Leigh, R. J. 2017. Air quality affected by trees in real street canyons: The case of Marylebone neighbourhood in central London. *Urban For Urban Gree*, *22*, 41–53.

Li, Z., Zhang, H., Juan, Y.-H., Lee, Y.-T., Wen, C.-Y., & Yang, A.-S. 2023a. Effects of urban tree planting on thermal comfort and air quality in the street canyon in a subtropical climate. *Sustainable Cities Soc.*, *91*, 104334.

Mochida, A., Tabata, Y., Iwata, T., & Yoshino, H. 2008. Examining tree canopy models for CFD prediction of wind environment at pedestrian level. *J. Wind Eng.*, *96*(10), 1667–1677.

Tominaga, Y., Wang, L. (Leon), Zhai, Z. (John), & Stathopoulos, T. 2023. Accuracy of CFD simulations in urban aerodynamics and microclimate: Progress and challenges. *Build. Environ.*, *243*, 110723.

Wilson, J. D. 1985. Numerical studies of flow through a windbreak. *J. Wind Eng.*, *21*(2), 119–154.

Xie, J., Liu, C.-H., Mo, Z., Huang, Y., & Mok, W.-C. 2020. Near-field dynamics and plume dispersion after an on-road truck: Implication to remote sensing. *Sci. Total Environ.*, *748*, 141211.

Xue, F., & Li, X. 2017. The impact of roadside trees on traffic released PM10 in urban street canyon: Aerodynamic and deposition effects. *Sustainable Cities Soc.*, *30*, 195–204.

Zhang, H., Qi, L., Wan, J., Musiu, E. M., Zhou, J., Lu, Z., & Wang, P. 2022. Numerical simulation of downwash airflow distribution inside tree canopies of an apple orchard from a multirotor unmanned aerial vehicle (UAV) sprayer. *Comput Electron Agr.*, *195*, 106817.

Zheng, X., & Yang, J. 2022. Impact of moving traffic on pollutant transport in street canyons under perpendicular winds: A CFD analysis using large-eddy simulations. *Sustainable Cities Soc.*, *82*, 103911.